Appl. Phys. A (2017) 123:674
DOI 10.1007/s00339-017-1280-z

Applied Physics A
Materials Science & Processing

Impact of liquid environment on femtosecond laser ablation

A. Kanitz[1] · J. S. Hoppius[1] · M. Fiebrandt[2] · P. Awakowicz[2] · C. Esen[1] · A. Ostendorf[1] · E. L. Gurevich[1]

Received: 25 August 2017 / Accepted: 22 September 2017 / Published online: 9 October 2017

Abstract The ablation rate by femtosecond laser processing of iron in different liquids is investigated for fluences up to 5 J/cm^2. The resulting fluence dependency is modeled by an approach derived from the two-temperature model. In our experiments, the liquid environment strongly affects the effective penetration depth, e.g, the ablation rate in water is almost ten times higher than in toluene. This effect is discussed and introduced phenomenologically into the model. Additional reflectivity measurements and plasma imaging provide improved insight into the ablation process.

1 Introduction

Ultrashort pulsed laser (USP) ablation is commonly used for precise material removal and modification [1]. Adding a liquid to the process improves the processing quality due to a smaller heat-affected zone and reduced re-deposition of debris [2, 3]. Another application is the production of nanoparticles directly into a liquid solution which offers a universal approach to synthesize a variety of different size-controlled nanomaterials [4–6].

Due to the complexity of the involved processes, e.g., the non-equilibrium electron energy distribution at short timescales [7, 8], the energy transfer of the electrons to the lattice [9, 10] and the interaction of hot material with the liquid surrounding [11, 12], USP-ablation in liquids remains a topic of intensive investigation delivering sometimes contradictory results. For example, increased [13] or decreased [14] ablation efficiency was reported.

A systematic and universal approach is needed to evaluate the ablation behavior in liquids and determine the highest ablation efficiency. In this paper, we focus on the influence of different liquids on the ablation rate.

Despite the fact that the ablation process in liquids is more complex than in vacuum or air, we use an approach that is established for the description of ablation behavior in vacuum [15–17] to analyze the ablation rate. This approach is derived from the two-temperature model (2TM) and only dependents on parameters of laser beam and target material. Thereby, it provides a framework on how to examine the ablation efficiency in liquids and underlying parameters such as different ablation regimes, effective ablation depth, and threshold behavior. In addition, we analyze the ablation crater morphology, employ fast ICCD-camera measurements to study the plasma evolution, and perform reflectivity measurements to examine the effect of the liquid on the absorptivity of the laser beam.

2 Materials and methods

Femtosecond laser pulses of 800 µJ pulse energy at central wavelength of 800 nm were used to ablate a crater by 300 single shots. The repetition rate was set to 1 Hz to minimize the influence of residual heat and screening effects [18–20]. The laser beam was guided through a galvo-scanner and an 80 mm telecentric lens onto the iron target. The pulse duration was measured before the scanner

✉ A. Kanitz
kanitz@lat.rub.de

[1] Applied Laser Technologies, Ruhr-Universität Bochum, Universitätsstr. 150, 44801 Bochum, Germany

[2] Institute for Electrical Engineering and Plasma Technology (AEPT), Ruhr-Universität Bochum, Universitätsstr. 150, 44801 Bochum, Germany

system at 35 fs. Thus, it is assumed that the pulse duration exceeds 35 fs, but remains in the femtosecond range. The applied fluence on the target surface was changed by moving the focal position. Thereby, the spot area changes allowing a careful adjustment of the fluence (see Fig. 1a). To avoid any influence and possible energy loss by an optical breakdown within the liquid [21], the target was always moved towards the focusing lens (compare Fig. 1a). The ablation rate was measured for fluences from 0.05 up to 5 J/cm^2. In our experiment, the spot diameter is larger than the ablation depth, and therefore, spot size-dependent effects are reduced. As target material, iron was chosen as due to its importance in science and technology. It consisted of 99.5% pure Fe sheets with a thickness of 0.5 mm and was placed in a glass vessel covered by the liquid with a height of 4 mm. Due to their common use and varying liquid properties as, for example, density, viscosity, and polarity, highly pure solutions of water, methanol, ethanol, acetone, and toluene were selected. The measurement uncertainty of the ablated volume measured by a white-light interferometer at the same experimental parameters was about 10%.

One fourfold camera system consisting of four coupled ICCDs with a gate time of 3 ns (PCO hfsc pro) was used to record the plasma evolution during the ablation process. The sequential images of the four cameras resulted in a total measurement time of 12 ns. The images were captured at an angle of 90° (compare Fig. 1b). The jitter of the camera and trigger system was in the range of one nanosecond. A ×10 objective and a shortpass edge filter resulted in an effective wavelength bandwidth from 400 to 750 nm. The sensitivity of the camera was kept constant for all conditions.

Figure 1c shows the experimental setup for reflectivity measurements. The iron target was placed at an angle of 45° to the laser beam. The reflected light was collimated by another 80 mm lens and guided onto a diffusing screen. The reflected power was measured by a fast photodiode ($\tau \sim 2$ ns). As these measurements only intend to show the relative change of reflectivity between the different liquids, the measured values have not been calibrated to find absolute reflectivity of the surface. Furthermore, the polarisation-dependent reflectivity on the incident angle of the laser beam differs around 10% and is, therefore, in the same order of magnitude as the experimental uncertainty.

3 Theory

Based on the investigations by Nolte et al. [22], a solution for the lattice temperature T_i can be deduced from the 2TM [23, 24] which is valid for ultrashort timescales:

$$T_\mathrm{i} \cong \frac{\Phi}{C_\mathrm{i}} \frac{1}{l^2 - \delta^2} \left[l\, exp(-\frac{z}{l}) - \delta\, exp(-\frac{z}{\delta}) \right]. \quad (1)$$

It takes into account that the resulting lattice temperature (compare Eq. 1) is related to the optical penetration depth δ and the electron-thermal penetration depth l due to electron heat conduction whereas C_i is the heat capacity of the lattice and Φ the applied fluence. For low fluences (< 1 J/cm^2) $\delta >> l$ dominates, while at high fluences, $\delta << l$ [8, 22, 25–27]. Usually, [1, 15, 28, 29], the case $\delta >> l$ with the effective penetration depth $L = \delta ln(\frac{\Phi}{\Phi_{\mathrm{th},\delta}})$ is used to describe the ablated volume ΔV as a function of fluence:

$$\Delta V = \frac{E_0}{2\Phi}\, \delta\, ln^2\left(\frac{\Phi}{\Phi_{th}}\right) \quad (2)$$

for a Gaussian beam with a fluence distribution $\Phi = \Phi_0\, exp(-r^2/\omega^2)$, with ω being the beam radius and $\Phi_0 = E_0/\pi\omega^2$ the peak fluence, Φ_th the threshold fluence, and E_0 the absorbed energy. The highest ablation efficiency is found at $\Phi = e^2\Phi_{\mathrm{th},\delta}$ which is directly related to the ablation threshold and relatively low compared to achievable fluences nowadays (< 1 J/cm^2). In this paper, we take both cases into account, such that Eq. 3 consists in a linear superposition of two processes dominating at $\delta >> l$ and $\delta << l$:

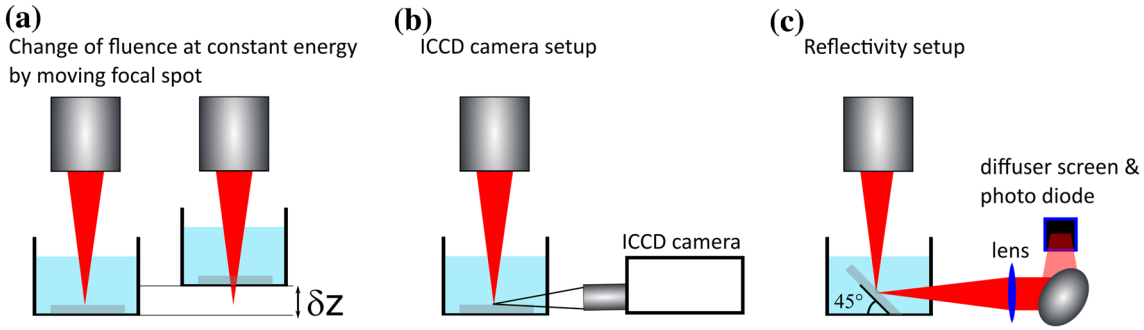

Fig. 1 Scheme of the different experimental setups: **a** illustration of the change of fluence by defocusing, **b** plasma imaging by a fourfold ICCD camera, and **c** reflectivity measurements with a photodiode

$$\Delta V = \frac{E_0}{2\Phi} ln\left(\frac{\Phi}{\Phi_{th,\delta}}\right)\left[A\delta ln\left(\frac{\Phi}{\Phi_{th,\delta}}\right) + Blln\left(\frac{\Phi}{\Phi_{th,l}}\right)\right] \quad (3)$$

with $\Phi_{th,\delta}$ and $\Phi_{th,l}$ being the threshold fluences regarding the two different penetration depths, respectively. As several mechanisms can influence the ablation rate in liquids and some are discussed in the last section of this paper, the constants A and B in Eq. 3 are introduced and will be determined from fits of the experimental data. The dimensionless constants A and B express the different weight between the impact of the optical and thermal penetration depths on the lattice heating. Note that this approximation by its nature overestimates $\Phi_{th,l}$ and underestimates B. However, it is convenient for the practical use, since a more precise description would require further assumptions about the physical nature and interaction of processes acting on the length scales δ and l within the metal. Another approximation for two competing processes, especially accounting for threshold values which lie closely together, was developed by Jaeggi et al. [17].

4 Results

Figure 2a displays the specific ablation rate ($\Delta V/E_0$) of iron in different liquids as a function of fluence up to 5 J/cm^2 measured by the ablated crater volume. The dashed lines represent fits according to Eq. 3. Note the good agreement between theory and experiment. The values of the fitted parameters are shown in Table 1.

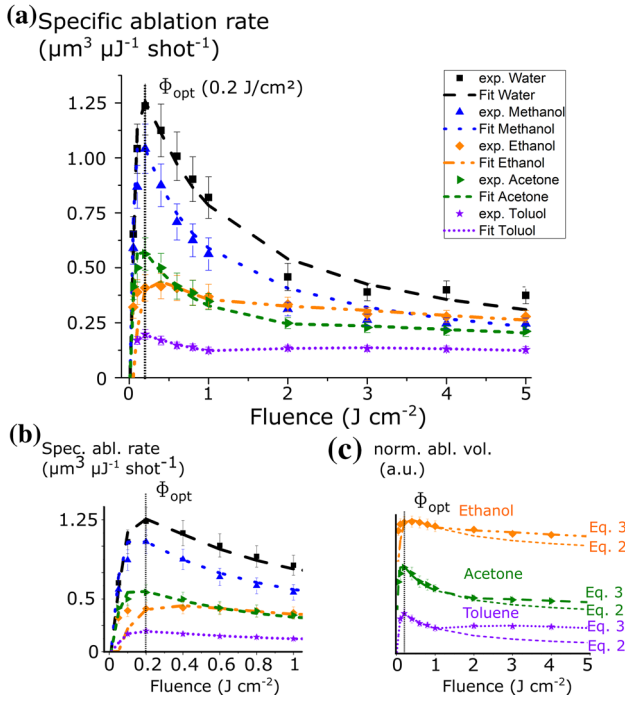

Fig. 2 Specific ablation rate of iron in different liquids **a** up to 5 J/cm^2, **b** up to 1 J/cm^2, and **c** normalized and shifted ablation rate of ethanol, acetone, and toluene fitted by different Eqs. 1 and 3 up to 5 J/cm^2

For fluences below 1 J/cm^2 (compare Fig. 2b), all experimental data points exhibit a similar dependency on the fluence. Only the total value of the ablated volume is significantly decreasing from water over methanol, acetone, and ethanol to toluene what is expressed by the decrease in the constant A, except for ethanol. The optimal ablation efficiency is found at Φ_{opt} = 0.2 J/cm^2 which means that the ablation threshold fluence is almost independent of the used liquid (as $\Phi_{th} = \Phi_{opt}e^{-2}$). This indicates that a change of chemical surface composition during the ablation by the liquid is negligible as this would considerably change its dependency on the fluence.

A more detailed analysis of crater topography at 0.2 J/cm^2 in different liquids shows that only the ablation depth is changed, while compared to the ablated volume, the spot diameter remains almost constant (see Fig. 3). Thus, the beam was not changed prior to the energy deposition, e.g., by white-light generation or self-focusing, as this would considerably alter the spot size. In sum for low fluences, only the first part of Eq. 3 is necessary, and therefore, the ablated volume can be described by Eq. 2. The phenomenologically introduced constant A describes the decrease in ablation depth observed in the experiments.

Above 1 J/cm^2, in acetone, ethanol, and toluene, the decline of the curve becomes less pronounced, e.g., in toluene, a plateau-like curve, is observed (compare Fig. 2c). Thus, the second part of Eq. 3 becomes apparent which is expressed by the increase in the constant B. Similar to low fluences, the constant B is related to the penetration depth. A more pronounced increase in ablation depth is found for the ablation in liquids in acetone, ethanol, and toluene. A direct comparison of the crater cross section of water and toluene at fluences of 0.2, 1 and 5 J/cm^2 shows that the relative increase is stronger in the case of toluene (see Fig. 4).

As mentioned afore, the ablation rate in toluene is reduced up to 85% compared to the ablation in water. This loss in ablation efficiency implies an effective energy loss

Table 1 Values of the fit parameters of the experimental values of the ablation rate in different liquids according to Eq. 3

Liquid	A	$\Phi_{th,\delta}$ (J/cm^2)	B	$\Phi_{th,l}$ (J/cm^2)
Water	9.4	0.024	0	-
Methanol	6.3	0.021	0	-
Ethanol	6.3	0.046	0.29	1.36
Acetone	3.5	0.020	0.42	1.77
Toluene	1.5	0.025	0.8	1.32

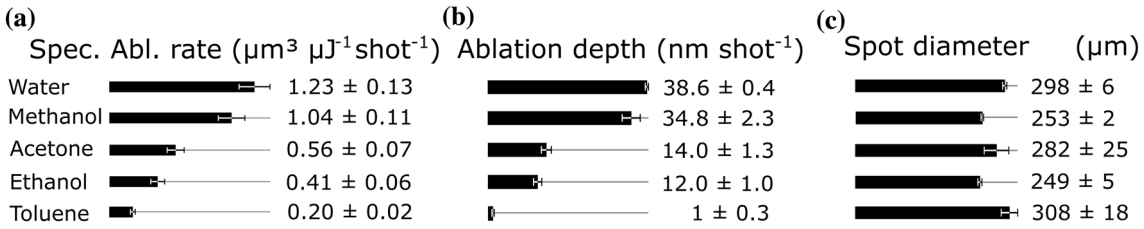

Fig. 3 **a** Specific ablation rate, **b** ablation depth, and **c** spot diameter of the ablation craters in different liquids at 0.2 J/cm^2

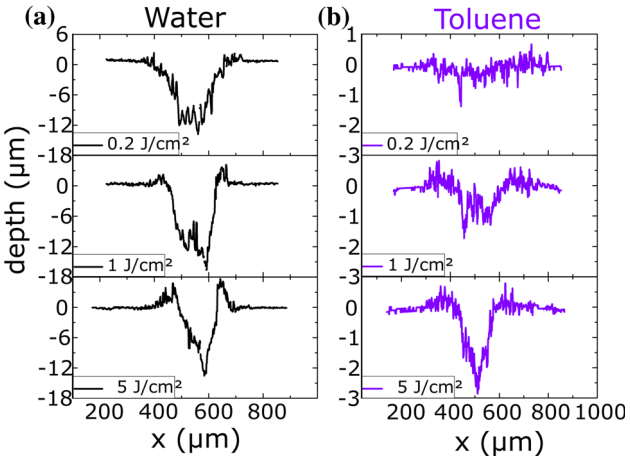

Fig. 4 Crater topography and cross section of ablation depth in **a** water and **b** toluene

during the ablation process. To reveal if the liquid surrounding changes the deposited pulse energy and thus the effective ablation depth, reflectivity measurements at 0.2 J/cm^2 were performed. As only a relative comparison is required, the measured values are normalized on the maximum value which was measured in toluene.

Figure 5 shows that the energy coupled onto the target is independent of the used liquid. The highest reflectivity is found in toluene and acetone. The maximal observed changes of reflectivity between the different liquids are 14%. These liquid-dependent changes of reflectivity can be caused by surface roughness or variation in refractive index (at the liquid boundaries), but do not correlate with the changed ablation rate. Thus, this result implies that the presence of the molecules in the liquid alters the ablation process at the stage *after* the energy deposition.

To obtain further information on the ablation process *after* the energy deposition, a fourfold ICCD-camera system was used for improved insight. Figure 6a shows the plasma evolution on four sequential ICCD images obtained during the ablation process. Typically, only image two and three (3 and 6 ns delay) of the sequence contained light emission showing that the emission lasted for only less than 6 ns and is, therefore, extremely short. This is in agreement with theoretical descriptions [30]. Shape and intensity of the emission do not differ significantly during the temporal evolution, a better understanding of plasma evolution requires an enhanced temporal resolution. However, these images show that the ablation plume is rapidly cooled down for fs-laser ablation in liquids. These short timescales rule out any fluorescence effect from the cavitation bubble, since optical transitions emit in the range of several tens of nanoseconds.

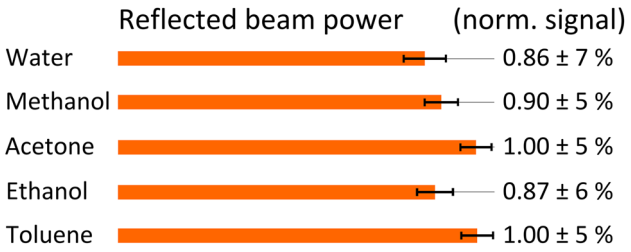

Fig. 5 Measurement of reflected power by a fast photo diode at 0.2 J/cm^2 (normalized on maximum measured value)

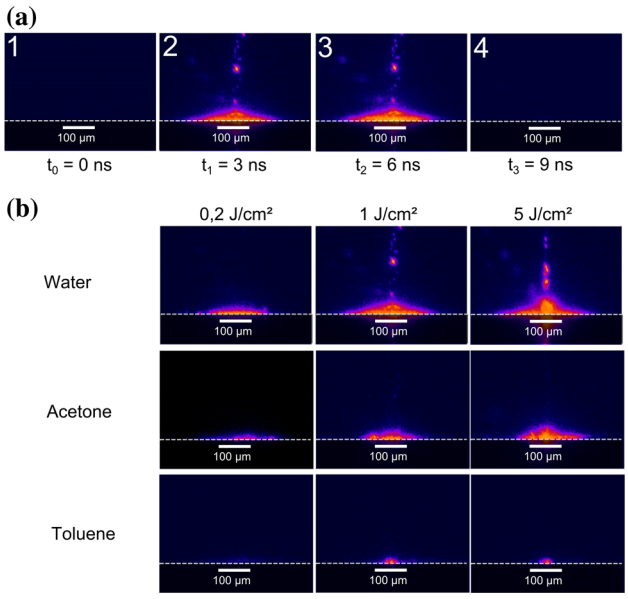

Fig. 6 **a** Temporal sequence (12 ns) of the plasma evolution (example of water at 1 J/cm^2). One image was taken with a gate time of 3 ns. **b** Single images in different liquids for laser fluences of 0.2, 1, and 5 J/cm^2 (example images taken at delay of 3 ns)

Figure 6b shows exemplarily the ICCD images for water, acetone, and toluene at different fluences. For all investigated liquids, the main plasma emission evolves from an almost flat and homogeneous plasma which is close to the surface at 0.2 J/cm^2 becoming more centrally located over 1 to 5 J/cm^2 in every liquid. Thus, the shape of emission intensity does not change significantly using different liquids and the different fluences are clearly distinguishable. Furthermore, spectral investigation by time-resolved echelle measurements showed a broad continuum for every liquid which was expected due to the short timescales; the plasma is present [31, 32] but without any additional information and is, therefore, not shown.

Our observations show that the strongest light intensity corresponds to the highest ablation rate. Thus, there are no indications that an enhanced plasma generation within the liquid by the laser beam impact caused the decrease in ablation rate.

5 Discussion

In order to discuss the ablation process and the fact that the effective ablation depth varies depending on the liquid, the generally accepted picture of ablation in liquids [12, 30, 33, 34] will be shortly reviewed:

The description of the ablation process of a submerged target is different than in air or vacuum. After the laser–matter interaction, where the photons transfer their energy to the electrons, the electrons transfer their energy to the phonons to heat up the lattice which is well described by the 2TM. By the quick heating, the metal transforms into an over-dense hot metal plasma which is ejected perpendicular to the surface as the ablation plume. Surrounded by the liquid medium, the ablation plume is confined close to the surface. The boundary of the liquid which is in contact with the ablation plume is quickly heated and subsequently vaporized. Continuous heating of this layer leads to high temperatures and pressures. These conditions drive the expansion of the layer to the growth of the cavitation bubble against the pressure exerted by the liquid.

Our results show that the fact that the electrons transfer their energy to the lattice holds valid, as our approach well describes the measured fluence dependency of the ablated volume. Our additionally obtained results by reflectivity measurements, and plasma imaging expand the insights into the ablation process in liquids.

As the spot size and reflectivity of the laser beam are independent of the used liquid, the ablation process is altered at the stage after the energy deposition. Thus, energy losses due to non-linear effects like self-focusing during beam propagation in the liquid medium or the creation of a nanometer thick plasma-mirror [35] which avoids penetration into the material are unlikely.

The ICCD-camera measurements further emphasize that an enhanced plasma generation, which would correlate with the ionization potential (compare Table 2), does not cause the decrease in ablation depth. In addition, the generated plasma is quenched almost an order of magnitude earlier than nanosecond-laser generated plasma [32].

Taking a closer look at the macroscopic properties of the liquids, which might lead to an enhanced confinement and thus, reduced ablation rate, most do not correlate with the observed decrease in ablation depth (e.g., density, viscosity, refractive index at 800 nm, surface tension, boiling temperature, heat capacity, vaporization enthalpy, reflectivity, or group velocity dispersion (see Table 2). Thus, shockwave [36, 37] and cavitation bubble [38], which depend on these parameters, are unlikely to have a major impact on the change of ablation rate. In fact, some of the correlation would even suggest a contradictory behavior during the ablation process. For example, the high-specific heat capacity of water would cool down the ablation process and reduce the ablation rate and the lower ionization potential of toluene should result in stronger plasma emission. Both features were not observed. Similar contradictory behavior on macroscopic material properties was observed by Streubel et al. [29] for PLAL in water for different target materials.

In sum, our approach accurately models the ablation behavior but the detailed mechanisms that lead to a reduction of effective ablation depth are unclear at the moment and require further investigation. For example, following an estimation by Bulgakova et al. [39], the characteristic collision time of electrons with molecules of the liquid at the metal–liquid interface is less than 1 fs, taking into account the density and cross sections for elastic scattering of the different liquids [40–43] and an estimated electron velocity of about 10^8 cm/s for electrons with a typical energy of some eV [44, 45]. Thus, there is a strong coupling between the electrons of the metal target at the surface and the adjacent molecules. This could lead to chemical reactions [46] or charging effects.

6 Conclusion

In conclusion, this paper investigates the influence of a liquid environment on femtosecond laser ablation of iron. Based on the 2TM, it provides a framework to examine the ablation efficiency and underlying parameters such as optimal ablation fluence, threshold value, ablation depth, and ablation regimes. Our experimental results show that the liquid has a significant impact on the effective ablation

depth. As, according to the 2TM, the effective ablation depth should only depend on the optical penetration depth, a target material parameter, additional reflectivity and plasma imaging experiments were carried out. Reflectivity measurements show that the ablation process leading to a change in effective ablation depth is altered at the stage after the energy deposition of the laser beam. Plasma imaging measurements show that the plasma is quenched in less than 6 ns and that the shape of the plasma emission reflects the applied fluence. Despite this additional measurements and further discussion on the influence of relevant physical and chemical macroscopic parameters of the liquid, the reason for the change of effective ablation depth in different liquids remains unclear.

Acknowledgements This work has been partially supported by the German Science Foundatin (DFG) within the research project GU1075/3. The authors gratefully acknowledge fruitful discussions with N. M. Bulgakova, D. Förster, J. Stähler, and C. Aroca. We gratefully acknowledge the support by A. Berger who made available the four ICCD camera setup.

Appendix

See Table 2.

Table 2 Macroscopic characteristics of used liquids

Liquid	Water	Methanol	Ethanol	Acetone	Toluene
ΔV, $\mu m^3 shot^{-1}$	1.24	1.04	0.41	0.56	0.20
ρ, g cm^{-1}	1.00	0.79	0.79	0.79	0.87
d	1.84	1.69	1.65	2.91	0.36
η, mPa s	1.00	1.20	0.59	0.32	0.59
σ, mN m^{-1}	72.9	22.4	22.5	25.2	28.4
c_p, kJ kg^{-1} K^{-1}	4.18	2.14	2.44	2.15	1.7
T_b, K	373	338	351	329	384
H, kJ kg^{-1}	2257	1104	841	539	351
E, kJ kg^{-1}	2500	2000	982	616	506
I, eV	12.6	10.8	10.4	9.7	8.8
M, a.m.u.	18	32	46	58	92
GVD, fs^2 m^{-1}	25	30	38	45	105
n	1.33	1.32	1.36	1.35	1.48
n_2, 10^{-20} m^2 W^{-1}	4.1–5.7	6.7	7.7	24	8.8

ΔV measured specific ablation rate at Φ_{opt}, ρ density, d - dipole moment, η viscosity, σ surface tension, c_p heat capacity at $T = 300$ K. T_b boiling point, H specific heat of evaporation, E specific energy needed to boil the liquid starting from room temperature, I ionzation potential, M molecular weight, GVD group velocity dispersion, n and n_2 linear and non-linear refractive index (according to [47–49])

References

1. B.N. Chichkov, C. Momma, S. Nolte, F. Alvensleben, A. Tünnermann, Appl. Phys. A **63**(2), 109 (1996). doi:10.1007/BF01567637
2. D. Zhang, B. Gökce, S. Sommer, R. Streubel, S. Barcikowski, Appl. Surf. Sci. (2016). doi:10.1016/j.apsusc.2016.01.071
3. A. Kruusing, Opt. Lasers Eng. **41**(2), 329 (2004). doi:10.1016/S0143-8166(02)00143-4
4. S. Barcikowski, G. Compagnini, Phys. Chem. Chem. Phys. **15**(9), 3022 (2013). doi:10.1039/c2cp90132c
5. D. Zhang, B. Gökce, S. Barcikowski, Chem. Rev. **117**(5), 3990 (2017). doi:10.1021/acs.chemrev.6b00468
6. A. Kanitz, J.S. Hoppius, M. Del Mar Sanz, M. Maicas, A. Ostendorf, E.L. Gurevich, Chemphyschem **18**(9), 1155 (2017). doi:10.1002/cphc.201601252
7. M. Lisowski, P.A. Loukakos, U. Bovensiepen, J. Stnhler, C. Gahl, M. Wolf, Appl. Phys. A **78**(2), 165 (2004). doi: 10.1007/s00339-003-2301-7
8. B.Y. Mueller, B. Rethfeld, Phys. Rev. B **87**(3) (2013). doi: 10.1103/PhysRevB.87.035139
9. D.S. Ivanov, V.P. Lipp, V.P. Veiko, E. Yakovlev, B. Rethfeld, M.E. Garcia, Appl. Phys. A **117**(4), 2133 (2014). doi:10.1007/s00339-014-8633-7
10. J. Byskov-Nielsen, J.M. Savolainen, M.S. Christensen, P. Balling, Appl. Phys. A **103**(2), 447 (2011). doi:10.1007/s00339-011-6363-7
11. M.V. Shugaev, C.Y. Shih, E.T. Karim, C. Wu, L.V. Zhigilei, Appl. Surf. Sci. **417**, 54–63 (2017). doi:10.1016/j.apsusc.2017.02.030
12. C.Y. Shih, C. Wu, M.V. Shugaev, L.V. Zhigilei, J. Coll. Interf. Sci. **489**, 3 (2017). doi:10.1016/j.jcis.2016.10.029
13. M.E. Shaheen, J.E. Gagnon, B.J. Fryer, J. Appl. Phys. **113**(21), 213106 (2013). doi:10.1063/1.4808455
14. S. Barcikowski, A. Hahn, A.V. Kabashin, B.N. Chichkov, Appl. Phys. A **87**(1), 47 (2007). doi:10.1007/s00339-006-3852-1
15. B. Neuenschwander, B. Jaeggi, M. Schmid, V. Rouffiange, P.E. Martin, in *SPIE LASE*, ed. by G. Hennig, X. Xu, B. Gu, Y. Nakata (International Society for Optics and Photonics, Bellingham, 2012)
16. J. Lopez, G. Mincuzzi, R. Devillard, Y. Zaouter, C. Hönninger, E. Mottay, R. Kling, J. Laser Appl. **27**(S2), S28008 (2015). doi:10.2351/1.4906479
17. B. Jaeggi, B. Neuenschwander, S. Remund, T. Kramer, SPIE Proc. **10091**, 100910J–1 (2017). doi:10.1117/12.2253696
18. P. Wagener, A. Schwenke, B.N. Chichkov, S. Barcikowski, J. Phys. Chem. C **114**(17), 7618 (2010). doi:10.1021/jp911243a
19. A. Kanitz, J.S. Hoppius, E.L. Gurevich, A. Ostendorf, Phys. Proc. **83**, 114 (2016)
20. M.R. Kalus, N. Bärsch, R. Streubel, E. Gökce, S. Barcikowski, B. Gökce, Phys. Chem. Chem. Phys. **19**(10), 7112 (2017)
21. A. Menéndez-Manjón, P. Wagener, S. Barcikowski, J. Phys. Chem. C **115**(12), 5108 (2011). doi:10.1021/jp109370q
22. S. Nolte, C. Momma, H. Jacobs, A. Tünnermann, B.N. Chichkov, B. Wellegehausen, H. Welling, J. Opt. Soc. Am. B **14**(10), 2716 (1997). doi:10.1364/JOSAB.14.002716
23. S.I. Anisimov, B. Rethfeld, in *Theory of ultrashort laser pulse interaction with a metal*, ed. by Sergei I. Anisimov and Baerbel Rethfeld (SPIE, 1997), pp. 192–203. doi: DOIurl10.1117/12.271674
24. L.V. Zhigilei, Z. Lin, D.S. Ivanov, The Journal of Physical Chemistry C **113**(27), 11892 (2009). doi:10.1021/jp902294m

25. P.B. Corkum, F. Brunel, N.K. Sherman, T. Srinivasan-Rao, Phys. Rev. Lett. **61**(25), 2886 (1988). doi:10.1103/PhysRevLett.61.2886
26. N.N. Nedialkov, S.E. Imamova, P.A. Atanasov, J. Phys. D **37**(4), 638 (2004). doi:10.1088/0022-3727/37/4/016
27. I. Mingareev, A. Horn, Appl. Phys. A **92**(4), 917 (2008). doi:10.1007/s00339-008-4562-7
28. B.H. Christensen, K. Vestentoft, P. Balling, Appl. Surf. Sc. **253**(15), 6347 (2007). doi:10.1016/j.apsusc.2007.01.045
29. R. Streubel, S. Barcikowski, B. Gökce, Opt. Lett. **41**(7), 1486 (2016). doi:10.1364/OL.41.001486
30. M.E. Povarnitsyn, T.E. Itina, P.R. Levashov, K.V. Khishchenko, Phys. chem. chem. phys. **15**(9), 3108 (2013). doi:10.1039/c2cp42650a
31. A. Tamura, A. Matsumoto, K. Fukami, N. Nishi, T. Sakka, J. Appl. Phys. **117**(17), 173304 (2015). doi:10.1063/1.4919729
32. A. De Giacomo, M. Dell'Aglio, R. Gaudiuso, S. Amoruso, O. De Pascale, Spectr. Acta B **78**, 1 (2012). doi:10.1016/j.sab.2012.10.003
33. M. DellAglio, R. Gaudiuso, O. De Pascale, A. De Giacomo, Appl. Surf. Sci. **348**, 4 (2015). doi:10.1016/j.apsusc.2015.01.082
34. C.Y. Shih, M.V. Shugaev, C. Wu, L.V. Zhigilei, J. Phys. Chem. C **121**(30), 16549 (2017). doi:10.1021/acs.jpcc.7b02301
35. C. Thaury, F. Quéré, J.P. Geindre, A. Levy, T. Ceccotti, P. Monot, M. Bougeard, F. Réau, P. d'Oliveira, P. Audebert, R. Marjoribanks, P. Martin, Nat. Phys. **3**(6), 424 (2007). doi:10.1038/nphys595
36. L.V. Zhigilei, D.S. Ivanov, Appl. Surf. Sci. **248**(1–4), 433 (2005). doi:10.1016/j.apsusc.2005.03.062
37. H. Hu, T. Liu, H. Zhai, Opt. Exp. **23**(2), 628 (2015). doi:10.1364/OE.23.000628
38. A. De Bonis, T. Lovaglio, A. Galasso, A. Santagata, R. Teghil, Appl. Surf. Sci. **353**, 433 (2015). doi:10.1016/j.apsusc.2015.06.145
39. N.M. Bulgakova, V.P. Zhukov, A.Y. Vorobyev, C. Guo, Appl. Phys. A **92**(4), 883 (2008). doi:10.1007/s00339-008-4568-1
40. M.T. Lee, de Souza, G L C, L.E. Machado, L.M. Brescansin, A.S. dos Santos, R.R. Lucchese, R.T. Sugohara, M.G.P. Homem, I.P. Sanches, I. Iga. J. Chem. Phys. **136**(11), 114311 (2012). doi:10.1063/1.3695211
41. J.R. Vacher, F. Jorand, N. Blin-Simiand, S. Pasquiers, Chem. Phys. Lett. **434**(4–6), 188 (2007). doi:10.1016/j.cplett.2006.12.014
42. Y. Itikawa, J. Phys. Chem. Ref. Data **34**(1), 1 (2005). doi:10.1063/1.1799251
43. M.G.P. Homem, I. Iga, J.R. Ferraz, A.S. dos Santos, L.E. Machado, de Souza, G. L. C., L.M. Brescansin, R.R. Lucchese, M.T. Lee, Phys. Rev. A **91**(1) (2015). DOI: 10.1103/PhysRevA.91.012713
44. W.S. Fann, R. Storz, H.W.K. Tom, J. Bokor, Phys. Rev. Lett. **68**(18), 2834 (1992). doi:10.1103/PhysRevLett.68.2834
45. C. Suarez, W.E. Bron, T. Juhasz, Phys. Rev. Lett. **75**(24), 4536 (1995). doi:10.1103/PhysRevLett.75.4536
46. C. Frischkorn, M. Wolf, Chem. Rev. **106**(10), 4207 (2006). doi:10.1021/cr050161r
47. E. Nibbering, M.A. Franco, B.S. Prade, G. Grillon, C. Le Blanc, A. Mysyrowicz, Opt. Comm. **119**(5–6), 479 (1995). doi:10.1016/0030-4018(95)00394-N
48. R.L. Sutherland, D.G. McLean, S. Kirkpatrick, *Handbook of nonlinear optics*, 2nd edn. (Marcel Dekker, New York, op. 2003)
49. S. Couris, M. Renard, O. Faucher, B. Lavorel, R. Chaux, E. Koudoumas, X. Michaut, Chem. Phys. Lett. **369**(3–4), 318 (2003). doi:10.1016/S0009-2614(02)02021-3